

## Catalytic Photooxidation of Pentachlorophenol using Semiconductor Nanoclusters

J.P. Wilcoxon

Nanostructures and Advanced Materials Chemistry, Dept 1152

Sandia National Labs

Albuquerque, N.M. 87185-1421

jpwilco@sandia.gov

RECEIVED  
MAY 04 2000  
OSTI**Abstract**

Pentachlorophenol (PCP) is a toxic chlorinated aromatic molecule widely used as a fungicide, a bactericide and a wood preservation, and thus ubiquitous in the environment. We report photo-oxidation of PCP using a variety of nanosize semiconductor metal oxides and sulfides in both aqueous and polar organic solvents and compare the photo-oxidation kinetics of these nanoclusters to widely studied bulk powders like Degussa P-25  $\text{TiO}_2$  and CdS. We study both the light intensity dependence of PCP photooxidation for nanosize  $\text{SnO}_2$  and the size dependence of PCP photooxidation for both nanosize  $\text{SnO}_2$  and  $\text{MoS}_2$ . We find an extremely strong size dependence for the latter which we attribute to its size-dependent band gap and the associated change in redox potentials due to quantum confinement of the hole-electron pair. We show that nanosize  $\text{MoS}_2$  with a diameter of  $d=3.0$  nm and an absorbance edge of  $\sim 450$  nm is a very effective photooxidation catalyst for complete PCP mineralization, even when using only visible light irradiation.

**Acknowledgment**

This work was supported jointly by the Division of Materials Sciences, Office of Basic Energy Sciences and the Energy Research/Environmental Management Program of the U.S. Department of Energy under contract DE-AC04-AL8500. Sandia is a multiprogram laboratory operated by Sandia Corporation, a Lockheed-Martin Company, for the U.S. Department of Energy.

## **DISCLAIMER**

**This report was prepared as an account of work sponsored by an agency of the United States Government. Neither the United States Government nor any agency thereof, nor any of their employees, make any warranty, express or implied, or assumes any legal liability or responsibility for the accuracy, completeness, or usefulness of any information, apparatus, product, or process disclosed, or represents that its use would not infringe privately owned rights. Reference herein to any specific commercial product, process, or service by trade name, trademark, manufacturer, or otherwise does not necessarily constitute or imply its endorsement, recommendation, or favoring by the United States Government or any agency thereof. The views and opinions of authors expressed herein do not necessarily state or reflect those of the United States Government or any agency thereof.**

## **DISCLAIMER**

**Portions of this document may be illegible in electronic image products. Images are produced from the best available original document.**

## I. Introduction

Contamination of sediments and aqueous water systems by halogenated organic compounds presents a serious environmental threat due to their toxicity and resistance to biodegradation. These chemicals are widely employed as pesticides, insecticides, and wood preservatives and thus are ubiquitous in the environment of both industrialized and agrarian nations. Even chemicals which have been banned for years, like DDT and its analogs, still pose major environmental threats and in fact, constitute the basis of several EPA superfund sites. A subgroup of these chemicals referred to as chlorinated aromatics includes chlorinated benzenes and biphenyls (PCBs), pentachlorophenol (PCP) and insecticides such as DDT.

PCP, the topic of this paper, is widely found in the environment, and it belongs to a family of chlorinated phenols that are among the most toxic chemicals known to man. In general, the more chlorines on the aromatic phenol ring the greater the biohazard. It has been postulated<sup>1</sup> that the widespread detection of PCP and its analogs in the environment may result from combustion, water treatment with chlorine in the presence of organic materials, and municipal sewage treatment plants and incinerators. Once discharged into the environment, these rather water insoluble compounds, (10-20 ppm in water, typically), seep into the sediment of rivers, lakes, and other bodies of water and continually leach out into the water supply, eventually affecting the entire mammalian food chain.

Microbial degradation and naturally occurring hydrolysis of these compounds is a very slow process (e.g. for 4-chlorophenol at 9 °C the half life is nearly 500 days).<sup>2</sup> Some direct photodegradation also occurs, though the limited optical absorbance of chlorinated aromatics above 350 nm in wavelength makes this process painfully slow. Sometimes this direct photolysis can actually lead to more toxic products (e.g. direct photolysis of PCP has been reported to lead to octachlorodibenzo-p-dioxin, an even more toxic species than its precursor).<sup>3</sup>

It is clear that more effective methods of treatment of these chlorinated aromatics must be sought. To this end, a few groups have been investigating photocatalytic oxidation of these compounds to form harmless CO<sub>2</sub> and HCl, a process referred to as total mineralization.<sup>2-4</sup> The semiconductor catalyst of choice in these studies has been TiO<sub>2</sub>, a white, photostable, non-toxic powder, whose principal deficiency is an absorbance edge which starts at about 385 nm, allowing less than 3% utilization of the solar spectrum.

It would be a major boon to have a visible light absorbing semi-conductor catalytic material available, which is also photostable and non-toxic. Such a photocatalyst would make it possible to exploit sunlight as the sole energy source required for detoxification. To this end we have employed our expertise in nanocluster synthesis and processing to make and purify

nanoparticles of MoS<sub>2</sub>, whose band-gap and absorbance edges can be adjusted by particle size based upon the quantum confinement of the hole-electron pair. In a recent paper we demonstrated the use of these new photocatalysts to destroy phenol, and demonstrated a strong effect of size or band-gap on the rate of photo-oxidation.<sup>5</sup>

In this paper we investigate the photooxidation kinetics and products formed for a standard material, Degussa P-25 TiO<sub>2</sub>, as compared to nanosize TiO<sub>2</sub>, SnO<sub>2</sub>, and MoS<sub>2</sub>. We examine the light intensity dependence for SnO<sub>2</sub> compared to TiO<sub>2</sub> (Degussa), and the effect of size on photooxidation kinetics for both SnO<sub>2</sub> and MoS<sub>2</sub>. We study photooxidation in aqueous systems and, for the first time, a system consisting almost entirely of a polar organic, acetonitrile.

## II. Materials Synthesis and Experimental Procedures

### Synthesis

In a previous paper describing the photooxidation of phenol, we gave details concerning the synthesis of nanosize MoS<sub>2</sub>.<sup>5</sup> The electronic and optical properties of this remarkable, structurally anisotropic, indirect bandgap semiconductor is discussed elsewhere.<sup>6-8</sup> Nanosize TiO<sub>2</sub> and SnO<sub>2</sub> were prepared by the controlled hydrolysis of the corresponding metal isopropoxide in isopropanol, and this general procedure has been described extensively by others in the literature.<sup>9,10</sup> We modified this general, acid-catalyzed metal alkoxide hydrolysis procedure by employing an aqueous solution of HCl at pH~1.5 which was slowly injected using a programmable syringe pump (KD Scientific Co., Model 100 pump) into a rapidly stirred titanium or tin isopropoxide (Aldrich Chemical) in isopropanol solution. It was discovered that both the pH and rate of addition of acid catalyst could be used to control the final size. In general we found that pH~2 or less was required to assure long term (i.e. weeks to months) colloidal stability against aggregation. The final (post-mix) ratio of water to isopropanol volumes was 10:1 in each case. In general, using higher pH values and slower mixing of the two solutions gave rise to larger nanoclusters as determined after 24 hours by dynamic light scattering (DLS). We were able to vary the size as measured by DLS from about 10 nm to 150 to 200 nm, but we were only interested in the 10-30 nm size regime for photocatalysis purposes. Table I gives further details of the nanocluster synthesis, nanocluster size, and physical properties.

Degussa P-25 TiO<sub>2</sub> was purchased from Degussa chemical company and used as received by making a stock solution of 10 mg/ml TiO<sub>2</sub> in milli-Q<sup>TM</sup> (Millicore Corp.) water. This stock solution was diluted as appropriate to achieve the desired catalyst concentration. No buffers or salts were added unless otherwise noted to any of our powder slurries or nanocluster solutions. CdS powder, 99.9% pure, ALFA chemicals, was similarly used as received and dissolved in milli-

Q water to make a standard 10 mg/ml solution which was then diluted for use in our photoreactor. Other powders investigated were also metals grade, purchased from ALFA and then made into stock slurries at 10 mg/ml. These stock solutions were used to prepared either 1 mg/ml or 0.1 mg/ml slurries in milli-Q™ water.

#### Purification/Processing of the Nanocatalysts

The as-synthesized MoS<sub>2</sub> nanoclusters were purified by extraction from the non-polar solution in which they were prepared, octane, into a water miscible but octane immiscible solvent, acetonitrile (ACN). The MoS<sub>2</sub> clusters in ACN were dried to a very small volume (e.g. ~0.5 ml) by centrifugal evaporation (~40x reduction in volume) using a Centrivap™ (Labconco Corp.) with a cold trap and then these reduced volume samples were added to water to form the catalyst solution.

Removal of ions and excess surfactants and isopropanol from the nanocluster solutions of MoS<sub>2</sub>, TiO<sub>2</sub>, and SnO<sub>2</sub> using the as-prepared solutions was achieved by dialysis using a 500 M.W. cut-off Spectra-Por™ (Spectrum Medical Industries, Inc.) dialysis membrane and dialysis against 1 liter of milli-Q water with one change over a 12-24 hour period. Some aggregation as determined by DLS of the MoS<sub>2</sub> and TiO<sub>2</sub> nanoclusters occurred under these conditions, but the catalytic activity improved substantially. The nanoclusters solutions were still visually transparent, stable without agitation, and non-turbid. All nanocluster catalyst solutions exhibited negligible light scattering in contrast to the control suspension of Degussa TiO<sub>2</sub> at a concentration of 0.1 mg/ml, which was milky white, cloudy, and exhibited intense multiple scattering. We note that the concentration of TiO<sub>2</sub> used in the present studies was about 16-20 times less than that used in most previous work, to try to minimize multiple scattering effects on the control catalyst. Even so, the intense multiple scattering characteristic of slurries of TiO<sub>2</sub> or CdS makes direct comparison of the quantum efficiency (Q.E.) of Degussa TiO<sub>2</sub> to the corresponding nanocluster solutions very difficult. Viable realistic approaches to address this issue have been discussed extensively in the literature.<sup>11</sup>

#### Catalyst Characterization

TEM and HRTEM were used to determine the nanocrystallinity of the materials, average cluster size, and polydispersity. The results were corroborated by use of DLS to measure the hydrodynamic diameter of the clusters in solution at the pH used for the photooxidation experiments. Except for nanosize TiO<sub>2</sub> this pH was ~4.0 (the typical pH of our deionized milli-Q™ water) and the solution was not buffered, nor purged with any gasses. It was necessary to keep the pH of the nanosize TiO<sub>2</sub> solutions at pH~2.0 to prevent aggregation. In the case of MoS<sub>2</sub>, the clusters were so small that TEM gives a better measure of cluster size than DLS, but

in the other cases the sizes reported were obtained from DLS which gives a better ensemble averaged size than TEM. Figure 1 shows a field of MoS<sub>2</sub> nanoclusters with an average size of  $d=3$  nm.

SAD has been used to determine that, for the case of nanoclusters of MoS<sub>2</sub> clusters large enough to give good electron diffraction (i.e.  $d>4.5$  nm), a crystal structure identical to bulk MoS<sub>2</sub> was observed.<sup>6</sup> Figure 2 shows XRD from a  $d=4.5$  nm MoS<sub>2</sub> solution dried to form a powder compared to data from a commercial MoS<sub>2</sub> (99.7%, Alfa) powder obtained on the same instrument. Except for the broadening due to the small domain size, the structures are identical. Further details concerning the optical properties and physical characterization of MoS<sub>2</sub> are given elsewhere.<sup>6</sup>

X-ray Fluorescence (XRF) spectroscopy (Spectrace QuantX<sup>TM</sup> system) was used to determine the inorganic composition of the purified, processed nanocluster solutions as well as to obtain the absolute metal concentrations indicated in later figures. Using XRF analysis, it was also possible to determine approximately the metal to sulfur ratio despite the notoriously low (~40 ppm) XRF sensitivity to low Z elements like S, and to compare this to bulk powders of MoS<sub>2</sub>. An example is shown in figure 3, where bulk MoS<sub>2</sub> powder is compared to nanocluster solutions of purified MoS<sub>2</sub>. In this figure we have indicated lines which arise from the cell windows and from the Ar present in the air environment. It was found that the ratio of Mo:S in our nanoclusters was ~1:2.5 to 1:3 showing some excess sulfur on the nanocluster surface which could not be removed by our purification procedures.

#### Catalyst Optical Properties

The optical absorbance properties of our nanocluster catalysts were determined using a Cary 2300 UV-visible-NIR spectrometer at the same concentrations used in the photooxidation studies. Slurries of Degussa TiO<sub>2</sub> in water were shaken and the spectrum rapidly obtained before powder settling occurred. The results of these absorbance measurements for nanosize TiO<sub>2</sub>, SnO<sub>2</sub>, MoS<sub>2</sub>, and the Degussa TiO<sub>2</sub> slurries are shown in figure 4. The strong multiple scattering of semi-opaque TiO<sub>2</sub> slurries even at 0.1 mg/ml in the 0.2 cm path length cell obscures the true band-edge absorbance of this material, which is clearly exhibited by the optically clear 20 nm diameter TiO<sub>2</sub> nanocluster solution. As can be observed in this figure, the TiO<sub>2</sub> slurry multiple scattering effectively enhances the absorbance probability of a photon in the relevant range of light output from our Xe arc lamp (300 to 400 nm) which corresponds to the actual TiO<sub>2</sub> absorbance (see the TiO<sub>2</sub>( $d=20$  nm) nanocluster absorbance curve). Light scattering is negligible for SnO<sub>2</sub>, MoS<sub>2</sub>, and TiO<sub>2</sub> nanocluster solutions and the absorbance curves of figure 4 represent pure absorbance for these solutions.

### PCP Optical Properties

To determine the optimum HPLC detector wavelengths to monitor the PCP concentration as a function of irradiation time, we first obtained the PCP absorbance spectrum at 10 ppm in water, methanol, and acetonitrile using our Cary 2300. These spectra are shown in figure 5. Note that the PCP absorbance is solvent dependent. This fact is important because the chromatography was run in an isocratic 70:30 MeOH:H<sub>2</sub>O ratio to optimize separation and peak shape, while still having an acceptably short run time for the metal oxide nanocatalysts. In the case of the MoS<sub>2</sub> nanoclusters the chromatography was performed in a solvent gradient from 70:30 ACN:H<sub>2</sub>O to 100% ACN over 20 minutes time to give good elution peak shape of the nanoclusters themselves. We find that the PCP absorbance under the mixed organic:H<sub>2</sub>O conditions most closely resembles the H<sub>2</sub>O absorbance shown below so we chose to obtain PCP concentrations based upon the absorbance at 325 nm, 250 nm, and 215 nm.

### Photooxidation Reactor

Our photooxidation reactor consists of a custom built (Ace Glassware Co.) cylindrical reactor with a flat glass base and an o-ring sealed quartz, Ace threaded<sup>TM</sup> window holder, with an aperture larger (~3 cm) than our collimated Xe lamp output beam, (~1.5 cm). The reactor has a total volume of about 60 ml, and we use 40 ml of liquid in all our reactions. The reactor has an o-ring sealed, Ace threaded<sup>TM</sup>, 45° side arm for liquid or gas phase sampling through a septa, if desired, but in all the studies to be described we simply removed the o-ring plug and sampled 0.6 ml of the sample at various irradiation times for analysis. This aliquot was filtered using an Hewlett-Packard HPLC filter (0.45 micron, cellulose) to remove suspended catalysts into a standard 2 ml crimp-top HP HPLC vial for either HPLC or GC/MS analysis. We tested to make sure no PCP was being adsorbed onto the filter. This filter allowed the nanosize catalysts to pass through and so we could simultaneously do HPLC analysis of the MoS<sub>2</sub> nanocluster catalysts.

We used a commercial 400 Watt Xe-arc lamp from Oriel . The output of this lamp is very close to that of the solar spectrum when combined with the 700 nm short-pass filter used. Overhead illumination of the cylindrical reactor is very advantageous since the flat bottom geometry of our cell allows rapid magnetic stirring of the catalyst solution - a vital aspect affecting the photooxidation rate of the powder slurries used as control catalysts. This stirring is unimportant for the nanosize catalysts, but for consistency we maintained the same rate for these catalysts too. In order to study only visible light photooxidation a 400 nm long-pass filter was also used to limit the incident irradiation wavelength, 1 to 400 nm <math>\lambda</math> <math><700\text{ nm}</math>. The lamp light output is monitored continuously by a Newport research (Newport Corp., Model 835) power meter with an IEEE-488 interface to a MacIntosh IICI computer, to track total irradiation time



and any power variations. The incident power was measured using the 1 cm<sup>2</sup> size calibrated photodiode probe from Newport research Corp. Neutral density filters on suprasil quartz substrates (Oriel Corp.) were used to attenuate the incident light by known amounts.

#### HPLC, GC/MS and Cl ion analysis of PCP Photooxidation Kinetics

To study the rate of photooxidation of PCP we used a HP 1050 High Pressure Liquid Chromatography (HPLC) system equipped with a photodiode array (PDA), a refractive index (RI), and a fluorescence (FL) detector(s). Unfortunately, the latter detector, though the ultimate in sensitivity for non-chlorinated aromatics like phenol, is nearly useless for PCP detection due to the quenching of the fluorescence by the chlorines on the aromatic ring of PCP. Never the less, we excited at 250 nm and detected fluorescence at 320 nm using this detector to detect any non-chlorinated aromatic by-products at the ppb level that might be formed during the photo-oxidation process. The entire spectrum from 200 nm (the solvent cut-off) to 600 nm is available at each time point in the elution peak chromatogram, but for quantitation purposes we chose to monitor at the three broad main features in the PCP spectrum shown in figure 5, 325 nm, 250 nm, and 215 nm. The latter wavelength gives the most sensitivity, while the former two can be used to avoid any detector saturation effects at high PCP concentrations and to check for consistency. Stock solutions of 10, 1, and 0.1 ppm PCP in milli-Q<sup>TM</sup> (Millicore Corp.) water were prepared and a linear detector response over this concentration range was verified. A minimum sensitivity of about 0.02 ppm was determined for absorbance at 215 nm. This is significantly better sensitivity than we could achieve using our HP 5890/5972 GC/MS even using selective ion monitoring.

Obtaining acceptable peak elution symmetry and retention time stability from a highly chlorinated aromatic like PCP is a very challenging chromatography problem. We found that using an HP analytical ODS200 column (reverse phase c18 terminated silica, 200 mm (length) by 4.6 mm (diameter) with 5 mm particle packing and 120 Å pores), and running a 60:40 or 70:30 Methanol (MeOH):H<sub>2</sub>O mobile phase mixture gave the best elution profiles, with good retention time stability over many runs. Various composition gradients of this mixture to 100% MeOH were also used to improve the separation if multiple organics were present. Using this solvent mixture it was also possible to detect the nanoclusters of MoS<sub>2</sub>, but we found that acetonitrile (ACN) gave more reproducibility for the nanocluster peak shape and elution time so a 60:40 ACN:H<sub>2</sub>O to 100% ACN was used in the MoS<sub>2</sub> nanocatalyst studies. This condition separates the nanoclusters, any surfactant, and PCP completely. We tried to use an independent column of the same type for the studies involving nanoclusters since some adsorption of the nanoclusters onto the column over many injections was found to alter the chromatographic elution behavior (i.e. peak shape, retention time) of the PCP, though not its quantitation (i.e. peak area). In all of

our studies we inject 50 ml of the 600 ml sample taken at a given time point in the irradiation, and analyze the area under the elution peak at the three monitoring wavelengths, taking the average as the concentration of PCP at that point in time.

Generally, because of the low concentrations and limited solubility of PCP in water (~20 ppm), it is not possible to use gas chromatography/mass spectroscopy (GC/MS) to directly identify unknown photooxidation byproducts observed in HPLC using ion fragmentation patterns in MS, so we purchased several putative photooxidation intermediate candidates like tetrachlorocatechol from Aldrich chemicals and ran HPLC on these chemicals under identical chromatography conditions as used in the PCP photooxidation experiments. This allowed us to identify any possible intermediates via retention time alone. We also had the luxury of the complete absorbance spectrum of each elution peak to identify whether a compound observed was aromatic or not. Never the less, we were not able to identify all intermediates positively and we never observed tetrachlorocatechol, a logical intermediate to be formed by OH radical attack on a Cl on the PCP ring. However, our inability to identify most intermediates was not a major problem as all these compounds were eventually completely mineralized themselves. Based upon the rate of appearance of these minor peaks compared to the rate of disappearance of the PCP peak, it was clear that these photooxidized compounds were not true intermediates on the pathway to complete mineralization, but rather, minor alternative photooxidation paths.

At the conclusion of several of the photooxidation reactions that were run long enough to achieve >99% disappearance of the PCP elution peak we used a Cl<sup>-</sup> selective electrode to determine [Cl]. We were able to verify that the expected amount of free chloride was generated as calculated from the initial concentration of 10 ppm PCP, so complete detoxification was accomplished with the best nanosize photocatalysts using only visible illumination as well as with nanosize SnO<sub>2</sub> and Degussa TiO<sub>2</sub> using full (UV + visible) lamp illumination. Because of the small reactor volume and large Cl electrode size, it was not possible to follow the [Cl] *in situ*.

### III. Experimental Results and Discussion

#### Direct Photolysis

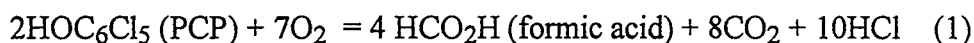
It is interesting to compare the results of direct photolysis of PCP with that observed with Degussa TiO<sub>2</sub>. In figure 6 we show the absorbance at 215 nm, A(215 nm) vs. elution time, t for different irradiation times using unfiltered Xe lamp illumination of PCP at 10 ppm in water. The products observed at the elution peaks of t=6.0 and t=3.27 minutes were not observed in the catalytic photooxidation experiments. We found that measurements of the [Cl] using a Cl selective electrode at t=480 minutes were consistent with nearly complete mineralization of the

PCP under direct photolysis. This contrasts with some claims that only toxic intermediates such as octachlorodibenzo-p-dioxin are formed under direct photolysis.<sup>12</sup> The UV-visible spectrum at  $t=6.0$  is not consistent with such a product formation.

Pelizzetti et al.<sup>13</sup> studied the direct photolysis of PCP starting from an initial concentration of 12.5 ppm at pH=3.0, and using a 1500 W Xe arc lamp with filters providing irradiation from 310 to 800 (conditions very similar to the present work except for the three fold increase in lamp intensity) and surprisingly observed a much slower rate of direct photolysis than we show in figure 7, even though their light intensity was more than 3 fold lamp greater than in the present work. This may be due to differences in reactor geometry.

### Catalytic Photooxidation

The generally accepted description of the complete mineralization of PCP in water is,



In previous work,<sup>14</sup> other intermediates in the complete reaction (1) included p-chlorinil ( $\text{C}_6\text{Cl}_4(=\text{O})_2$ ) or its reduced form. However, detection of this compound is difficult due to its low optical extinction coefficient in water. Also, this compound is reported to be unstable when stored in water and must be extracted into ether to allow detection by HPLC, so we did not expect to observe this compound. We also did not monitor the  $\text{CO}_2$  or formic acid concentrations because of the limited reactor volume we employed. However, our [Cl] measurement at completion (i.e. >99.9% PCP removal)  $t \sim 480$  minutes was consistent with the stoichiometry described in (1).

When Degussa  $\text{TiO}_2$  is added to the water at a concentration of 0.1 mg/ml the absorbance at 215 nm ( $A(215 \text{ nm})$  chromatograms) shows different reaction by-products than observed in direct photolysis, figure 6. In fact, we observe different by-products for each type of catalytic material we examined,  $\text{TiO}_2$ ,  $\text{SnO}_2$ , and  $\text{MoS}_2$ .

In figure 7 we show the results for catalytic photooxidation of PCP using Degussa P-25  $\text{TiO}_2$  at a concentration of 0.1 mg/ml in milli-Q water. There is less build up of intermediates than observed in the direct photolysis results of figure 6. The elution peaks at  $t=7.6$  and  $t=5.8$  are also destroyed more rapidly. Also, the photooxidation kinetics are significantly accelerated with the photocatalyst present.

Our observations of the increase in photooxidation rates with  $\text{TiO}_2$  compared to direct photolysis are consistent with other work using Degussa P25.<sup>1,14</sup> Since our reactor geometry, initial concentrations, and catalyst concentrations are significantly different from previous work a direct comparison with these other studies is difficult. However, our conditions are most similar

to those employed by Mills et. al.<sup>14</sup> in which a 450 W Xe arc lamp with IR cut-off filter was used and an initial concentration of 1.2 ppm was employed with 0.2 mg/ml of Degussa TiO<sub>2</sub> catalyst. They reported that complete mineralization was achieved under these conditions in about 3 hours, consistent with our results taking into account our 8-fold larger concentration of PCP.

Our photocatalytic oxidation results using nanosize SnO<sub>2</sub> are shown in figure 8.(bulk SnO<sub>2</sub> is nearly inactive for PCP photocatalysis). Here we observe breakdown products more similar to that of the direct photolysis results of figure 6, but with accelerated kinetics. No peak at  $t=7.6$  minutes is observed.

Nanosize SnO<sub>2</sub> has not been studied previously so these results cannot be compared directly to previous experiments. However, the rate of disappearance is comparable to that observed from Degussa TiO<sub>2</sub>. Since SnO<sub>2</sub> is cheaper than TiO<sub>2</sub>, but is ineffective as a bulk photocatalyst, these results are encouraging as they provide evidence that a robust metal oxide material in nanosize form can be competitive with Degussa TiO<sub>2</sub> slurries.

By integrating the areas observed in figures 6-8 and similar data collected for the other nanocluster catalysts studied one can obtain the kinetics behavior shown in figure 9. There are obviously dramatically different rates of photooxidation of PCP for these various metal oxides. As has been found by many others, Degussa P-25 has remarkable catalytic activity compared to nanosize TiO<sub>2</sub> (d=20 nm). Two additional things can be immediately noted from this figure. The first is that the photooxidation kinetics of TiO<sub>2</sub> powder is non-exponential, while both nanosized SnO<sub>2</sub> solutions, the TiO<sub>2</sub> nanocluster solution, and the direct photolysis kinetics are nearly exponential. Secondly, though initially Degussa TiO<sub>2</sub> is more active than the SnO<sub>2</sub> nanoclusters, they all reach >99% complete mineralization in ~8 hrs.

In previous work by Mills et. al.,<sup>14</sup> the kinetics of photooxidation using Degussa P-25 TiO<sub>2</sub> at 0.2 mg/ml was observed to be 0<sup>th</sup> order in [PCP] for [PCP]>0.6 ppm. In contrast, Barbeni et al.<sup>1</sup> showed first order behavior and an exponential decrease in [PCP] with irradiation time. Our results for both direct photolysis and to a lesser extent photocatalysis using Degussa TiO<sub>2</sub> and nanosize TiO<sub>2</sub> and SnO<sub>2</sub> also show an exponential decrease with time. However, the higher concentrations of TiO<sub>2</sub> used by previous workers and the resulting stronger multiple scattering may make previous determinations of the true kinetics ambiguous, as we show in our light intensity studies.

The apparently faster rate of photooxidation using Degussa P25 TiO<sub>2</sub> compared to the other materials is partly due to its intense multiple scattering of light which serves to confine the incident photons more effectively in the reactor. In other words, its *effective* absorbance cross-section is larger. The other nanosize photocatalyst solutions, being transparent, are somewhat

light intensity limited at the 0.1 mg/ml or less nanocatalyst concentrations employed in these studies. This effect is illustrated most easily by comparison of the light intensity dependence of Degussa TiO<sub>2</sub> vs. nanosize SnO<sub>2</sub> as we do in the next section of this paper.

It appears from Figure 9 as if the larger sized, d=58 nm SnO<sub>2</sub> nanoclusters are slightly more effective for photo-oxidation of the PCP than the smaller d=25 nm SnO<sub>2</sub> nanoclusters, both at 0.1 mg/ml concentration. However, this inference is probably incorrect when one considers the results shown in figure 10. We have run the PCP photooxidation reaction with the incident intensity reduced 10 fold in this case to see if photons are the "limiting reagent" in the nanocatalyst case but not in the TiO<sub>2</sub> slurry suspension case.. In the latter case, the intense multiple scattering effectively increases the light path of the incident photons and thus their absorbance probability and so there are many more photons available than are needed for the reaction at the full lamp light intensity, 250 mW/cm<sup>2</sup>. Thus, even when the photon intensity is reduced by an order of magnitude the slurry reaction doesn't slow proportionally, and the reaction kinetics are clearly not exponential under either of these conditions. However, under these irradiation conditions the nanocluster solutions are "starved" for photons and do slow down in a proportional fashion and do not exhibit an exponential decrease in [PCP] with time.

We observe that there is no difference in photocatalytic oxidation activity for the two sizes of SnO<sub>2</sub> nanoclusters under these lower light level conditions. From this observation we can conclude that an increase in specific surface area alone is not enough to accelerate the kinetics for nanoclusters in this colloidal size range. This observation contrasts markedly from that described below for smaller nanoclusters of MoS<sub>2</sub>, where a very strong size dependence is observed due to quantum confinement effects.

#### Effect of Incident Light Intensity On Photooxidation Kinetics

Because of the strong light dependence demonstrated in figure 9 & 10, we undertook a systematic investigation of the incident light intensity dependence of nanosize SnO<sub>2</sub> compared to Degussa TiO<sub>2</sub> powder slurries. We did not attempt to make a similar comparison in the case of nanosize MoS<sub>2</sub> because of the significant difference in the absorbance edges of TiO<sub>2</sub> and nanosize MoS<sub>2</sub>.

Figure 11 shows the change in photooxidation rate of PCP using a slurry of 0.1 mg/ml Degussa TiO<sub>2</sub> over a range of incident intensities of  $I_0 = 250 \text{ mW/cm}^2$  (no light attenuation) to  $I = 0.01 I_0$ . We were initially surprised by the very weak dependence of the kinetics on the incident intensity in the range  $0.1 I_0 < I < I_0$ . Apparently, due to extreme confinement of the light in the reactor due to multiple scattering from the slurry suspension, there are more than enough photons available so the reaction acts as if it is nearly zero order in the light intensity. Note that only when the light intensity is reduced by about a factor of 100-fold does the kinetics

of PCP photooxidation become exponential, as is the case with all the nanosize photocatalysts investigated. Therefore, one should really be comparing the PCP photooxidation kinetics for nanosize  $\text{TiO}_2$  and  $\text{SnO}_2$  to slurries of  $\text{TiO}_2$  in this light intensity regime. Unfortunately, this intensity is at least 2 orders of magnitude lower than has been previously investigated using Degussa  $\text{TiO}_2$  and any organic.

Contrast the behavior shown in figure 11 by the slurry suspension of  $\text{TiO}_2$  to that exhibited by a nanocluster solution of  $\text{SnO}_2$  using the same reactor geometry and irradiation conditions. The results of this experiment are shown in figure 12. The same exponential PCP oxidation kinetics were observed for the nanosize  $\text{TiO}_2$ (d=20 nm),  $\text{SnO}_2$ (d=25 nm),  $\text{SnO}_2$ (d=58 nm), and  $\text{MoS}_2$ (d=4.5nm). For each of the non-scattering nanocluster solutions we observe a rate that is roughly proportional to the incident light intensity, and the PCP oxidation kinetics appears exponential (i.e. first order in [PCP]) over the entire light intensity range investigated.

#### Other Powder Slurries

It has been demonstrated that certain materials, when prepared as semi-conductor photoelectrodes, are effective photo-electrochemical catalysts.<sup>15</sup> The best known example of this is  $\text{RuO}_2$  which has been deposited on colloidal  $\text{TiO}_2$  enhancing the rate of water photo-oxidation substantially.<sup>15</sup> We were interested in seeing if bulk powders of this, and other similar materials would provide good photooxidation catalysts for organics like PCP. Our results on two of these materials, formulated as slurry suspensions in milli-Q water are shown in figure 13. The powders were the highest grade purity available, obtained from ALFA chemicals. The results are rather surprising, showing that these materials actually reduced the rate of normal photolysis and essentially acted as "anti-oxidation agents", preserving the PCP. We found this also to be true of bulk powders of  $\text{MoS}_2$ ,  $\text{WO}_3$ , and  $\text{SnO}_2$ . The mechanism of this effect is quite mysterious, but does indicate that the presence of suspended, micron size, inorganic materials may substantially decrease the rate of photooxidation of organic pollutants. This effect deserves more extensive examination, but does emphasize the remarkably rapid rates of photo-oxidation we observe in nanosize semiconductors as illustrated in figure 12 above. It is interesting to note that  $\text{PtS}_2$  has the same layered hexagonal structure found in  $\text{MoS}_2$ , and in bulk form is very ineffective as a bulk photocatalyst as is bulk  $\text{MoS}_2$  powder, probably due to having too narrow a bandgap. As we will see, nanosize  $\text{MoS}_2$  with its substantially wider gap is very effective as a photocatalyst.

#### Photooxidation of PCP in polar, non-aqueous solvents

It has been postulated that photooxidation of organic materials using semiconductors in water requires the presence of OH radicals generated from the water to proceed at any appreciable rate.<sup>13</sup> Furthermore, many researchers deliberately aerate their photocatalyst suspensions in order to optimize the photooxidation process, and claims have been made

numerous times that nearly total quenching of the photooxidation process occurs when inert gas purging is employed.<sup>1</sup> Thus, the use of aprotic organic solvents should cause a severe quenching of the photooxidation due both to the lack of OH radicals and reduced oxygen levels because of reduced gas solubility.

It is thought that direct hole transfer from a semiconductor photocatalyst is rare and oxidation typically occurs via an OH radical trapped by the photo-induced hole on the semiconductor surface. To establish this hypothesis isopropyl alcohol is sometimes added to the reactor to quench the reactive products produced via OH radical oxidations, leaving only direct valence band hole transfer products to be observed. We reasoned that if the presence of water and high levels of oxygen gas is critical to the photooxidation of PCP that performing the reaction in a polar aprotic organic solvent like acetonitrile (ACN) would effectively inhibit the photooxidation of PCP, since such solvents solvate significantly lower amounts of molecular oxygen. To provide for some source of OH radicals we did add 1%/vol of deaerated H<sub>2</sub>O to the ACN solution. We were somewhat skeptical about the central role of OH radicals in the photooxidation mechanism of PCP anyway, due to our failure to observe any catechol intermediates, such as we<sup>5</sup> and others<sup>16</sup> have observed in phenol photooxidation studies using HPLC.

Figure 14 shows a study of the effect of solvent on the photooxidation of PCP both in direct photolysis (no catalyst) and using Degussa TiO<sub>2</sub> at 0.1 mg/ml. As observed in this figure, though the rate of photooxidation is 2-5x slower in ACN, photocatalysis does occur indicating the mechanism for PCP photooxidation is water and in ACN is similar. This is verified by the presence of the same  $t=7.6$  minute elution peak (see figure 2) representing a photooxidation intermediate in the HPLC chromatogram for both solvents. As stated earlier this intermediate is not a catechol (i.e. the product of OH radical attack on a Cl on the aromatic ring). In ACN, it is a larger peak which is more slowly broken down when compared to water, however. This shows there are subtle differences in the photooxidation mechanism for the two solvents. The important conclusion from this experiment is that the presence large amounts of H<sub>2</sub>O is not critical for the photooxidation of PCP. It would be interesting to extend these experiments to a wider range of organic chemicals, solvents, and photocatalysts to test the generality of our results.

#### Effect of surfactants and salts on PCP photooxidation

In many real world situations, there are both multiple organic pollutants, inorganic salts, and even surfactants present in the water. Very little research is available in the literature comparing the effects of these complexities on the photooxidation kinetics, and nothing is known concerning their effects on PCP photooxidation. Thus, we examined separately the effect of a

simple, common salt, NaCl, and a common type of organic, water soluble surfactant, a quaternary ammonium salt, dodecyltrimethylammonium chloride (DTAC) on the photooxidation kinetics. We selected this surfactant for investigation since we use it to stabilize nanosize MoS<sub>2</sub> against aggregation, and because it has the common counterion, Cl, for comparison to NaCl, so we can separate out the effect of Cl from that of the organic dodecyltrimethylammonium entity.

The results of our investigations are summarized in figure 15, for a single catalyst, Degussa P-25 TiO<sub>2</sub> in water at 0.1 mg/ml under 300 nm <math>\lambda</math> <math>< 700</math> nm irradiation from our 400 W Xe arc lamp. We first observe that even low levels of NaCl have a poisoning effect on the catalyst, though it is mild in this case. Similar observations have been made in field tests of TiO<sub>2</sub> where diionization of the aqueous waste stream have been found to be necessary.<sup>17</sup> In the laboratory, Barbeni et. al.<sup>1</sup> reported no inhibition by NaCl at  $1 \times 10^{-3}$  M, so it appears that it is inhibitory only at the higher levels investigated here.

We expected the role of surfactants to be inhibitory - blocking access to surface sites on the semiconductor. However, our surprising observation is the significant acceleration of the photooxidation of PCP in the presence of the surfactant DTAC. We made similar observations of enhanced photooxidation rates in the case of nanosize MoS<sub>2</sub> and SnO<sub>2</sub>. Clearly, the surfactant does not serve to block key surface sites as we expected. Instead it somehow aids the electron and/or hole transfer process. It is interesting to note that the use of a structurally similar surfactant, dodecyltrimethylammonium bromide (DTAB), also accelerates the photooxidation process, though not as much as DTAC, and that these observed increases in photooxidation rate are also seen using ACN as a solvent. So the counterion, Br or Cl, in the polar head group of the surfactant is important. It is important to note that the HPLC elution peak corresponding to surfactant DTAC does not change in position or area, showing that these surfactants are robust compared to PCP during photooxidation. These types of multicomponent experiments are worth extending to other organic chemicals like 4-chlorophenol, or phenol, due to the unexpected positive effects of the presence of these cationic surfactants.

#### Photooxidation of PCP using nanosize MoS<sub>2</sub> and visible irradiation.

In addition to the difficulties noted above in comparing transparent solutions of nanoclusters of TiO<sub>2</sub> or SnO<sub>2</sub> to strongly multiply scattering slurry suspensions of TiO<sub>2</sub>, in the case of nanosize MoS<sub>2</sub> we also have qualitatively different absorbance characteristics between these oxide and sulfide materials, which render direct comparison of the photooxidation kinetics of our de facto standard, Degussa P-25, to nanosize MoS<sub>2</sub> impossible. Basically, the problem is that under illumination using a 400 nm long-pass filter, TiO<sub>2</sub> has no activity, as expected, since it doesn't absorb light in the 400 nm <math>\lambda</math> <math>< 700</math> nm region. So, for purposes of comparison to a bulk material suspension, we chose to use a metals grade CdS bulk powder (ALFA), whose



absorbance onset of 525 nm is similar to that of nanosize MoS<sub>2</sub>, and which, unlike TiO<sub>2</sub>, does exhibit some photooxidation activity using 400 nm <  $\lambda$  < 700 nm irradiation.

Figure 16 shows the relative PCP concentration vs. time for two sizes of MoS<sub>2</sub> nanoclusters compared to CdS. The concentration of each MoS<sub>2</sub> solution as determined by XRF is shown in the figure, and it should be noted that due to some losses during the MoS<sub>2</sub> purification/dialysis, the concentrations are less than that of the CdS slurry suspensions. All other reaction conditions were identical.

Measurements of PCP concentration vs. irradiation time by HPLC using a 70:30 ACN:H<sub>2</sub>O to 100% ACN gradient elution allowed us to also determine the concentration of the surfactant-stabilized MoS<sub>2</sub> nanoclusters while we observed the destruction of the PCP. It was necessary to use ACN instead of MeOH as the organic component in these experiments to get good, reproducible HPLC of the nanoclusters. However, the HPLC peak symmetry of the PCP was not as good under these conditions, so we analyzed the irradiated samples using both methods. We confirmed that the MoS<sub>2</sub> nanocluster elution peak area and corresponding optical spectrum of the nanoclusters under visible irradiation showed no changes with irradiation time, demonstrating that the MoS<sub>2</sub> nanoclusters were acting as true photocatalysts. There seemed to be no substantial improvement in the MoS<sub>2</sub> nanocluster photooxidation kinetics when full lamp (300 nm <  $\lambda$  < 700 nm) was used. This result is not surprising given the relatively strong visible absorbance of both sizes of MoS<sub>2</sub> nanoclusters shown in figure 3 coupled with the small lamp output below 400 nm.

Figure 16 demonstrates the dramatic effect of nanocluster size in the strong quantum confinement regime on PCP photooxidation kinetics. The change in size in this regime, it must be remembered, affects both the electronic valence and conduction band energy levels shifting them to more favorable values with decreasing size. Adding to the complexity of a direct comparison of the size effect in MoS<sub>2</sub> to that of control catalysts such as Degussa P25 TiO<sub>2</sub> is the larger surface area and change in relative number of Mo edge sites with decreasing size. The key observation, never-the-less, is that both d=4.5 and d=3.0 nm MoS<sub>2</sub> are substantially more active than CdS, though this slurry suspension effectively absorbs a substantially larger amount of incident light than the nearly transparent (i.e. non-scattering) MoS<sub>2</sub> solutions. It should also be noted, that though we did not perform a detailed study of the effect of nanocatalyst concentration on PCP photooxidation kinetics, this effect is weak (almost linear) for nanoclusters in the 0.01 to 0.1 mg/ml range due to the low PCP concentrations used (10 ppm). Our opinion is that the dramatic differences observed in the rates of photooxidation of PCP by d=3.0 MoS<sub>2</sub> at 0.09 mg/ml and d=4.5 mg/ml d=4.5 MoS<sub>2</sub> at 0.036 mg/ml, is due primarily to the wider bandgap of the former nanoclusters. This is because d=4.5 nm MoS<sub>2</sub> with an absorbance onset of nearly

600 nm absorbs substantially more of the visible light than the  $d=3.0$  nm  $\text{MoS}_2$  solution, with an absorbance onset of about 450 nm. It is worth noting that the PCP photooxidation kinetics curve terminates at  $t=120$  minutes for the case of  $d=3.0$  nm  $\text{MoS}_2$  simply because the next point measured at  $t=240$  minutes showed no detectable PCP (i.e. less than 20 ppb)! By way of *very indirect* comparison, this is significantly better PCP photooxidation than is achieved using Degussa P-25  $\text{TiO}_2$  and *full lamp irradiation* (i.e.  $300 \text{ nm} < \lambda < 700 \text{ nm}$ )!

Another strong argument favoring the effect of energy level shifts compared to a simple increase in surface area with decreasing size on the photooxidation kinetics is our observation of nearly identical photooxidation rates for  $d=26$  nm and  $d=58$  nm  $\text{SnO}_2$  nanoclusters. These  $\text{SnO}_2$  sizes are much too large to affect valance and conduction band levels due to quantum confinement, yet the increase in specific surface area (total area/gram of catalyst) is very significant (almost 4x), about the same as that expected for the two sizes of much smaller  $\text{MoS}_2$  nanoclusters!

We also examined our  $d=8-10$  nm  $\text{MoS}_2$  nanoclusters employed in previous studies of phenol photooxidation<sup>5</sup> using visible irradiation and found very little activity, showing how important the quantum confinement and concomitant energy levels shifts are on the positive results of figure 17.  $\text{MoS}_2$  in the 8-10 nm size range absorbs intensely throughout the visible range  $400 \text{ nm} < \lambda < 700 \text{ nm}$ , but has a very small shift in the valence or conduction band levels relative to the bulk.<sup>8</sup> Although its specific surface area is admittedly considerably lower, ( $\sim 10x$ ), this area reduction is not sufficient to explain its lack of activity.

#### IV. Conclusions

Using HPLC analysis we showed that the product intermediates in the photooxidation of PCP depend on whether a photocatalyst is used and also on the material type of the catalyst. Nanosize  $\text{SnO}_2$ , for example, gave different products than powders of Degussa  $\text{TiO}_2$  or nanosize  $\text{MoS}_2$ .

We demonstrated a poisoning effect upon addition of a simple salt,  $\text{NaCl}$ , to slurries of  $\text{TiO}_2$ . More surprisingly, we observed that certain cationic surfactants actually enhance the activity of  $\text{TiO}_2$  slurries and the degree of enhancement depended on the counterion,  $\text{Cl}$  or  $\text{Br}$ . Furthermore, HPLC showed that these cationic surfactants themselves were not photooxidized.

We also investigated the kinetics of PCP photooxidation as a function of light intensity comparing nanosize  $\text{SnO}_2$  and  $\text{TiO}_2$  to slurries of  $\text{TiO}_2$ . We showed that a fair comparison of the activity of these materials requires an investigation of the kinetics in light intensity regimes where the reaction is first order in PCP. For slurry systems, the intense multiple light scattering

inherently increases the light collection efficiency of the reactor giving rise to an almost negligible dependence of the PCP photooxidation rate on the light intensity in the regime  $25 \text{ mW/cm}^2 < I_0 < 250 \text{ mW/cm}^2$ . In this same intensity regime nanosize  $\text{SnO}_2$  shows a proportional reduction with decreasing light intensity and first order kinetics in  $[\text{PCP}]$  demonstrating that photons are a limiting "reagent" for these nanosize materials at the  $[\text{PCP}]$  typically found in the environment (1-10 ppm).

We made the first studies of PCP photooxidation using slurries of  $\text{TiO}_2$  and nanosize  $\text{SnO}_2$  in a polar organic solvent, ACN containing 1%  $\text{H}_2\text{O}$ . Surprisingly, we found significant, though reduced compared to pure  $\text{H}_2\text{O}$ , photocatalytic activity for both types of catalysts, despite the much lower  $\text{O}_2$  and  $\text{H}_2\text{O}$  levels. This may indicate the role of hydroxyl radicals is not as critical in the total mineralization process as other researchers have suggested. It also indicates these photocatalysts will function adequately in aqueous systems containing a significant amount of miscible organic solvents.

In the case of nanosize  $\text{SnO}_2$  we observed little or no size dependence of the photooxidation rate on size when comparing  $d=25 \text{ nm}$  to  $d=58 \text{ nm}$   $\text{SnO}_2$  colloids at the same mass concentration. Thus, it appears having larger available surface area, by itself, does not make this material more active.

The very strong  $\text{MoS}_2$  size dependence we observe for this complex PCP photooxidation experiment is consistent with that observed for simpler photoredox reactions we have previously performed using time-resolved fluorescence to follow the electron transfer (E.T.) rates.<sup>8</sup> In these experiments we observed a dramatic reduction of E.T. rates to bipyridine and substituted bipyridine molecules as a function of increasing cluster size. It is also consistent with the strong size dependence we previously observed<sup>5</sup> in the visible light driven photocatalysis of phenol, where  $d=8\text{-}10 \text{ nm}$   $\text{MoS}_2$  had negligible activity while  $d=4.5 \text{ nm}$   $\text{MoS}_2$  was active.

**References.**

- (1) Barbeni, M.; Pramauro, E.; Pelizzetti, E. *Chemosphere* **1985**, *14*, 195.
- (2) Hoffmann, M.R.; Martin, S.T.; Choi, W.; Bahnemann, D.W.; *Chem. Rev.* **1995**, *95*, 69.
- (3) Mills, A.; Davies, R.H.; Worsley, D.; *Chem. Soc. Rev.* **1993**, 417.
- (4) Serpone, N.; Maruthamuthu, P.; Pickat, P.; Pelizzetti, E.; Hidaka, H.; *J. of Photochem. Photo. A: Chem.* **1995**, *85*, 247.
- (5) Thurston, T.R.; Wilcoxon, J.P.; *J. Phys. Chem* **1998**, *103*, 11.
- (6) Wilcoxon, J.P.; Newcomer, P.; Samara, G.A.; *J. Appl. Phys.* **1997**, *81*, 7934.
- (7) Tributsch, H.; *Z. Naturforsch.* **1977**, *32a*, 972.
- (8) Parsapour, F.; Kelley, D.F.; Craft, S.; Wilcoxon, J.P.; *J. Chem. Phys.* **1996**, *104*, 1.
- (9) Kiwi, J; Borgarello, E; Duonghong, D; Gratzel, M.; *Stud. Surf. Sci. Catal.* **1983**, *16*, 135.
- (10) Jean, H.; Ring, T.A.; *Langmuir* **1986**, *2*, 251.
- (11) Serpone, N.; Terzian, R.; Lawless, D.; Kennipohl, P.; Sauve, G.; *J. Photochem. Photobiol: A: Chem.* **1993**, *73*, 11.
- (12) Plimmer, J.R.; Knliengebiel, U.I.; Crosby, D.G.; Wong, A.S.; *Advan. Chem. Ser.* **1973**, *120*, 44.
- (13) Pelizzetti, E.; Barbeni, M.; Pramauro, E.; Serpone, N.; Borgarello, E.; Jamieson, A.; Hidaka, H.; *La Chmica E L'Industria* **1985**, *67*, 623.
- (14) Mills, G.; Hoffmann, M.R.; *Environ. Sci. Technol.* **1993**, *27*, 1681.
- (15) A. Hagfeldt, A.; Gratzel, M.; *Chem. Rev.* **1995**, *95*, 49.
- (16) Serpone, N.; *Res. Chem. Intermed.* **1994**, *20*, 953.
- (17) Crittenden, J.C.; Zhang, Y.; Hand, D.W.; Perram, D.L.; Marchard, E.G.; *Water Envir. Res.* **1996**, *68(3)*, 270.

## Tables

**Table I. Synthetic Details for Catalysts used in Photoxidation Studies**

Sample Name	Surfactant/Solvent	Precursor/concentration/	Sulfiding or Hydrolysis Agent	Rate of Mixing (ml/min)	pH (final)
SnO <sub>2</sub> (d=25 nm)	Isopropanol	Sn(Isopropoxide)/50 mg/ml	HCl@pH=1.5	0.1 ml/min	2
SnO <sub>2</sub> (d=58 nm)	Isopropanol	Sn(Isopropoxide)/25 mg/ml	HCl@pH=1.5	0.01 ml/min	2
TiO <sub>2</sub> #28(d=20 nm)	Isopropanol	Ti(Isopropoxide)/50 mg/ml	HCl@pH=1.5	0.1 ml/min	2
TiO <sub>2</sub> #10(d=55 nm)	Isopropanol	Ti(Isopropoxide)/25 mg/ml	HCl@pH=1.5	0.01 ml/min	2
MoS <sub>2</sub> (d=3.0)	DTAC(8%)/c6OH(11%)/c8	MoCl <sub>4</sub> /0.002M	H <sub>2</sub> S(.01M)	N.A.	N.A.
MoS <sub>2</sub> (d=4.5)	DTAB(8%)/c6OH(11%)/c8	MoCl <sub>4</sub> /0.002M	H <sub>2</sub> S(.01M)	N.A.	N.A.
MoS <sub>2</sub> (d=8-10)	DTAB((1%)/c6OH(1.5%)/c8	MoCl <sub>4</sub> /0.002M	H <sub>2</sub> S(.01M)	N.A.	N.A.

DTAC = Dodecyltrimethylammonium Chloride (Fluka Chemicals, 99%)

DTAB = Dodecyltrimethylammonium Bromide (Fluka Chemicals, 99%)

## Figure Captions

Figure 1. TEM of a field of  $d=3.0$  MoS<sub>2</sub> nanoclusters prepared by evaporation from acetonitrile onto a holey carbon grid.

Figure 2. XRD from a  $d=4.5$  dried, nanocrystalline powder (dotted line) compared to a bulk powder of MoS<sub>2</sub> (solid line).

Figure 3. XRF lines from high purity MoS<sub>2</sub> bulk powder are co-plotted with purified nanosize MoS<sub>2</sub>. Both Mo Ka and S Ka lines are shown.

Figure 4. UV-Visible absorbance spectra of nanocatalysts and control bulk powder (Degussa P-25, TiO<sub>2</sub>) are shown. All concentrations were 0.1 mg/ml.

Figure 5. UV-Visible absorbance spectra of PCP in three common HPLC solvents., water, methanol (MeOH), and acetonitrile (ACN).

Figure 6. Direct photolysis of PCP in water is followed by the absorbance monitored by a PDA at 215 nm,  $A(215 \text{ nm})$  vs. elution time,  $t$ . Note that the by-products observed at  $t=6.0$  and  $t=3.27$  minutes only appear after nearly complete disappearance of the PCP. The chromatograms for different irradiation times are off-set for clarity.

Figure 7. Catalytic photooxidation of PCP in water containing 0.1 mg/ml Degussa P25 TiO<sub>2</sub> is followed by the absorbance monitored by a PDA using the optical absorbance at 215 nm,  $A(215 \text{ nm})$  vs. elution time  $t$ . Note the by-products observed at  $t=7.6$  minutes absent from of figure 6. The direct photolysis by-product at 5.8 minutes is observed, however.

Figure 8. Catalytic photooxidation of PCP in water containing 0.1 mg/ml  $d=28 \text{ nm}$ , SnO<sub>2</sub> is followed by the absorbance monitored by a PDA whose absorbance at 215 nm,  $A(215 \text{ nm})$  is plotted vs. elution time,  $t$ . Note the absence of the  $t=7.6$  byproduct of figure 7 and the formation of the by-products observed in direct photolysis of figure 6 at  $t=5.90$  and  $t=3.31$  minutes.

Figure 9. Normalized PCP concentration vs. irradiation time using a 400 W Xe arc lamp with  $300 \text{ nm} < \lambda < 700 \text{ nm}$  irradiation. Initial PCP concentration was 10 ppm in all cases, and the incident light intensity was  $250 \text{ mW/cm}^2$ .

Figure 10. Relative concentration of PCP vs. irradiation time for several nanocluster metal oxide catalysts using 10-fold attenuated incident light intensity  $I=0.1 I_0 = 25 \text{ mW/cm}^2$ .

Figure 11. Relative PCP concentration (all initial concentrations were 10 ppm in water) vs. irradiation time using a 400 W Xe arc lamp with the  $300 \text{ nm} < \lambda < 700 \text{ nm}$  pass filters and measured incident intensity of  $I_0=250 \text{ mW/cm}^2$ , and using Degussa P25 TiO<sub>2</sub> at 0.1 mg/ml.

Figure 12. Relative PCP concentration (all initial concentrations were 10 ppm in water) vs. irradiation time using a 400 W Xe arc lamp with the  $300 \text{ nm} < \lambda < 700 \text{ nm}$  pass filters and a

measured incident intensity of  $I_0 = 250 \text{ mW/cm}^2$ , and using nanosize,  $d = 26 \text{ nm}$   $\text{SnO}_2$  at  $0.1 \text{ mg/ml}$ .

Figure 13. Relative PCP concentration (10 ppm in  $\text{H}_2\text{O}$  at  $t=0$ ) vs. irradiation time using a Xe arc lamp with  $I_0 = 250 \text{ mW/cm}^2$  for no catalyst,  $\text{RuO}_2$  and  $\text{PtS}_2$  powders at  $0.1 \text{ mg/ml}$ .

Figure 14. Relative PCP concentration (10 ppm at  $t=0$ ) vs. irradiation time using a Xe arc lamp with  $I_0 = 250 \text{ mW/cm}^2$  for no catalyst, and Degussa  $\text{TiO}_2$  powder at  $0.1 \text{ mg/ml}$  in two solvents, milli-Q water and acetonitrile (ACN) containing 1 vol% water.

Figure 15. Relative PCP concentration (10 ppm initially in water) vs. irradiation time. The effect of inorganic ions and surfactants on the photooxidation kinetics of PCP in water is shown.

Figure 16. Relative PCP concentration in water vs. irradiation time using a 400 W Xe arc with long and short pass filters allowing only  $400 \text{ nm} < \lambda < 700 \text{ nm}$  to reach the stirred solutions.

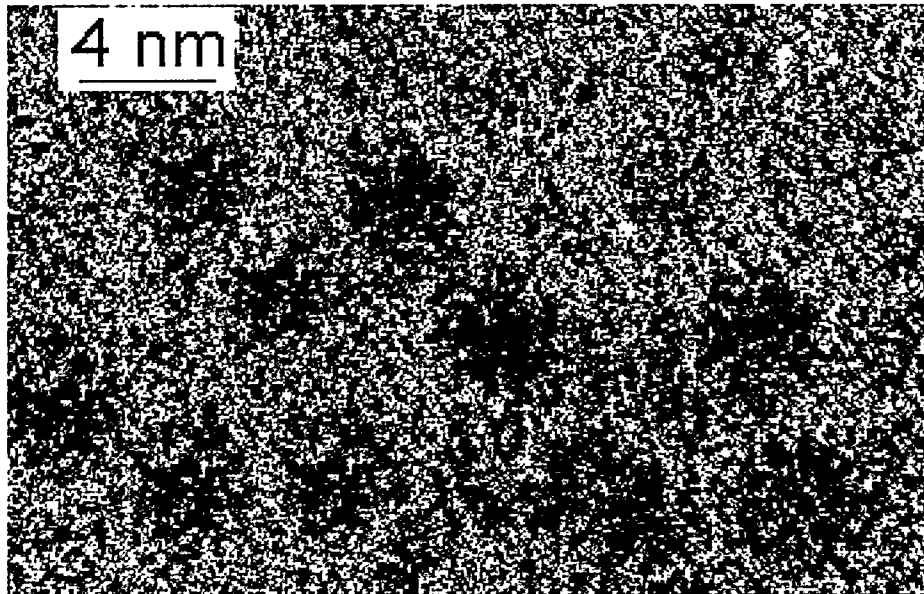
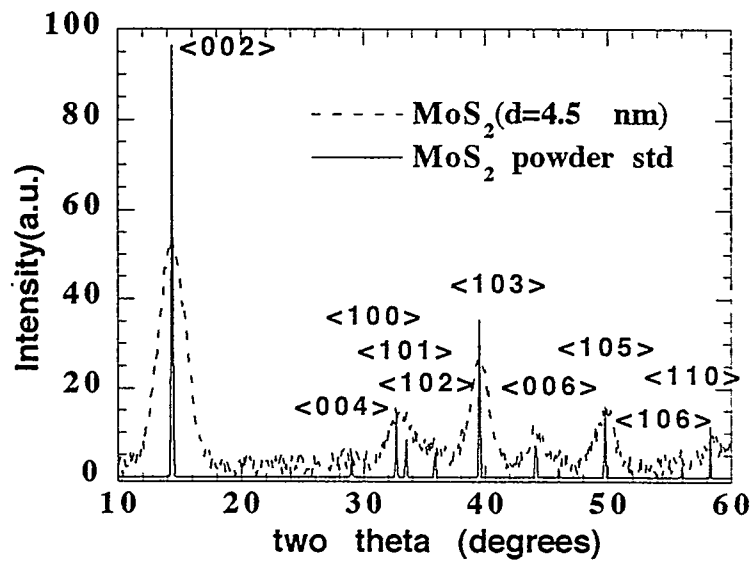
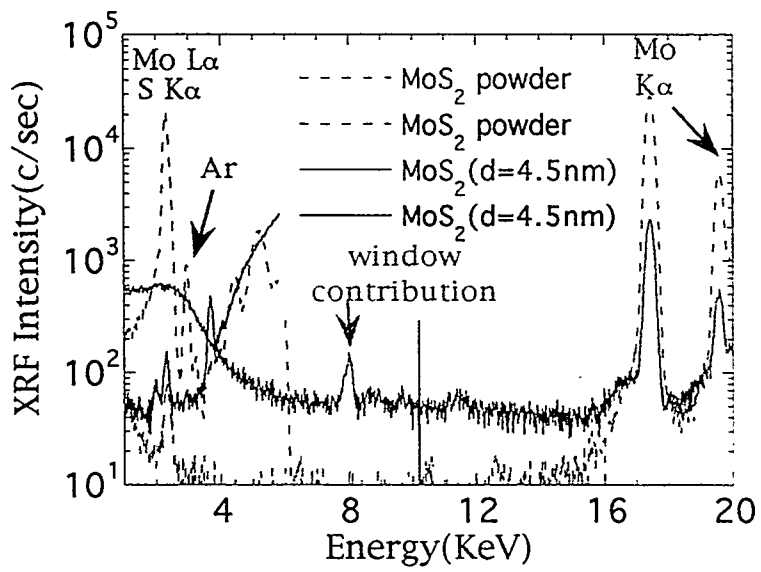


fig 1, Wilcoxon et al.

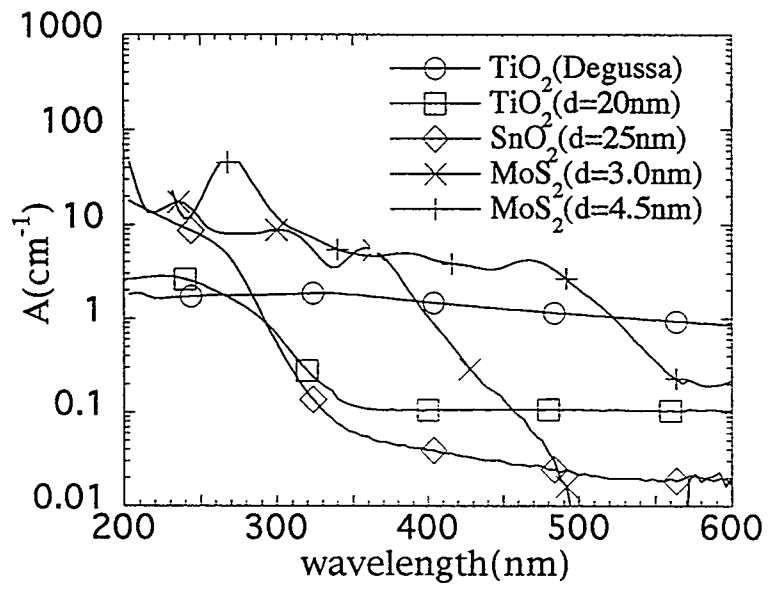




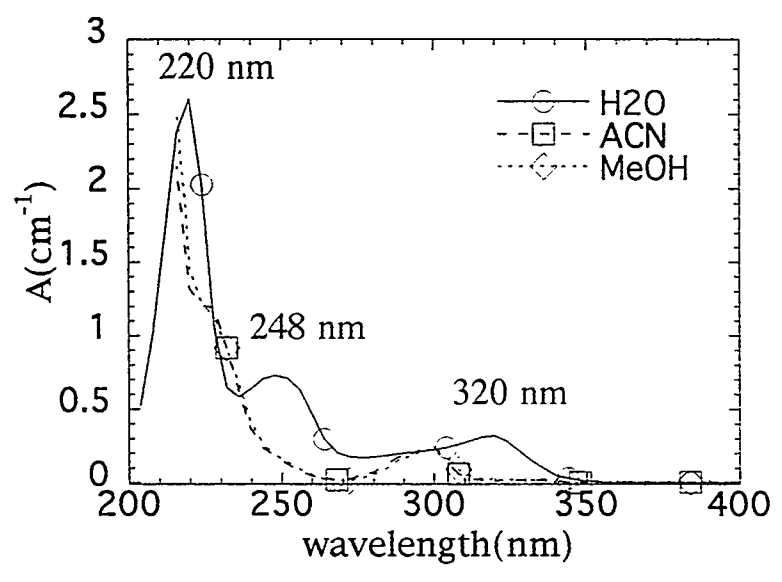
Ullmann, Fig. 3

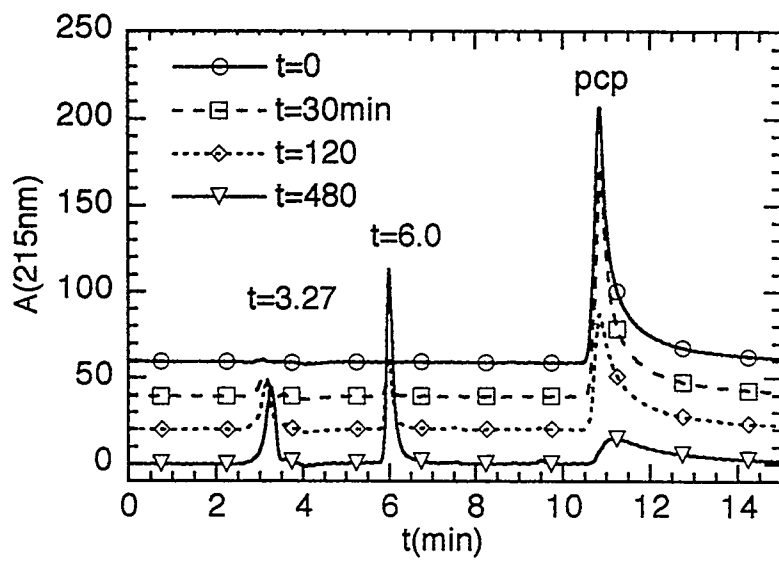


Wilcoxon, Fig. 4

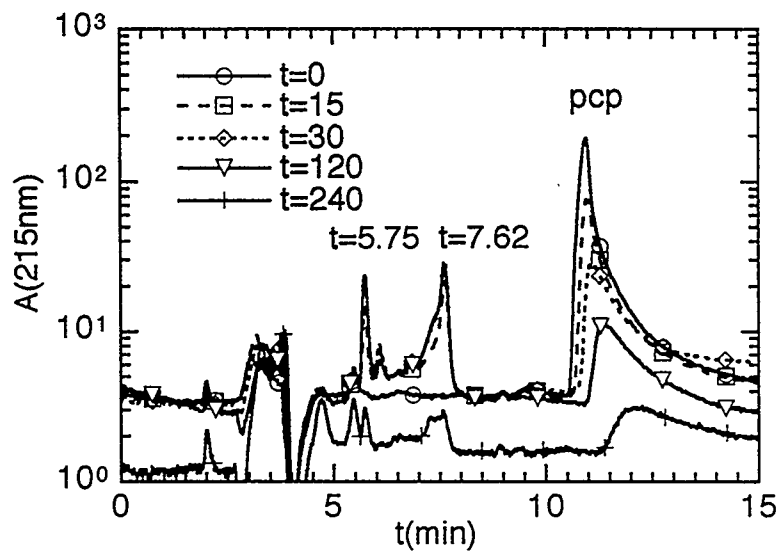


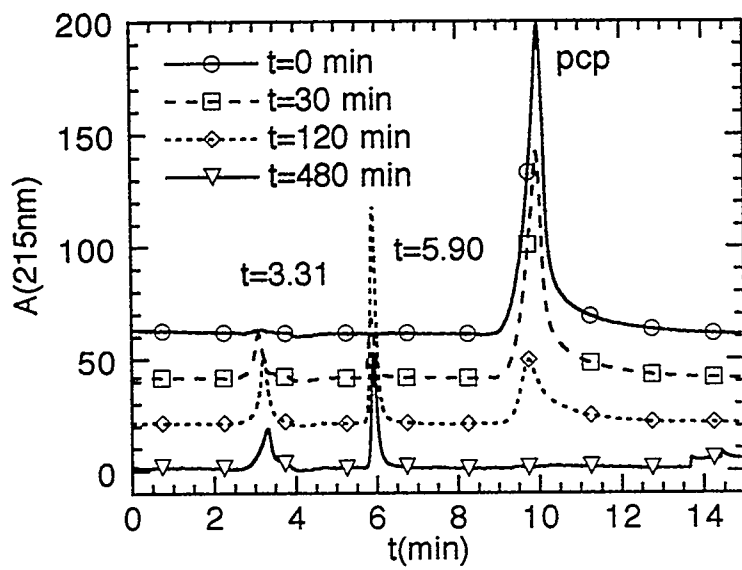
Wilcox, Fig. 5



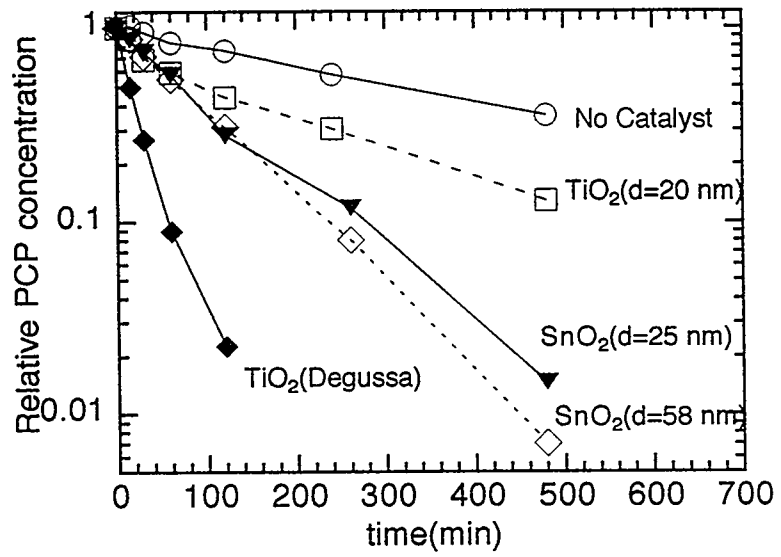


Wilcoxon, Fig 7



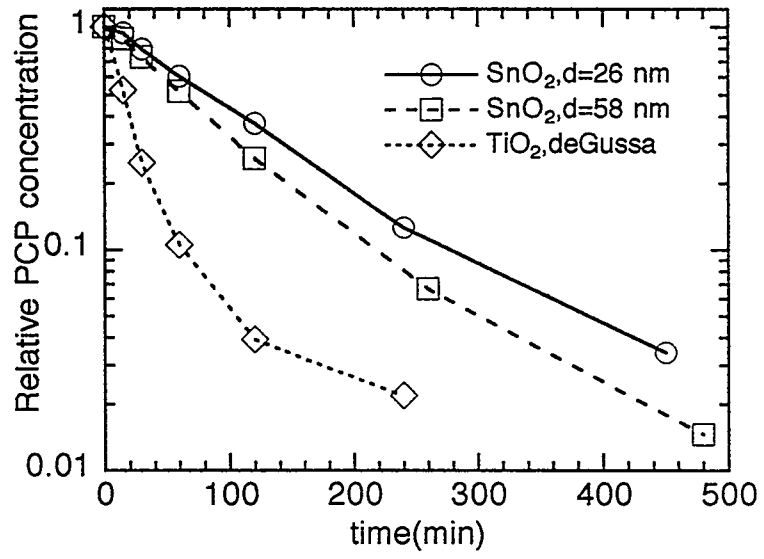


Wilcoxon, Fig 9

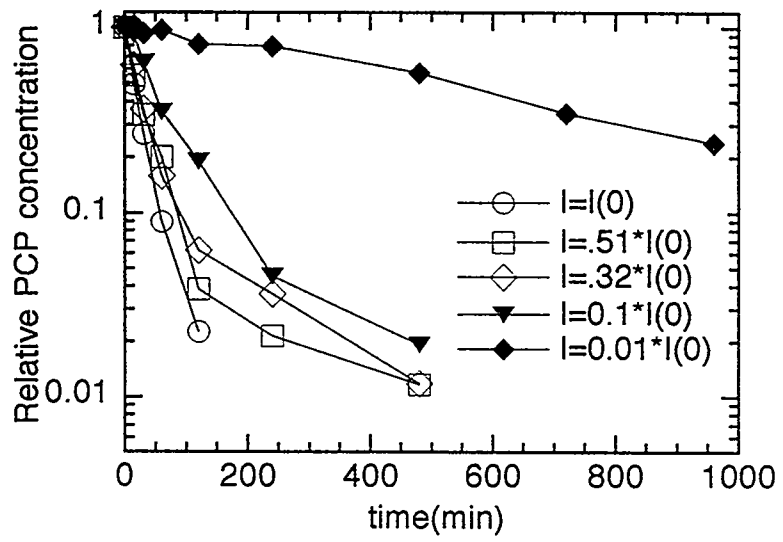




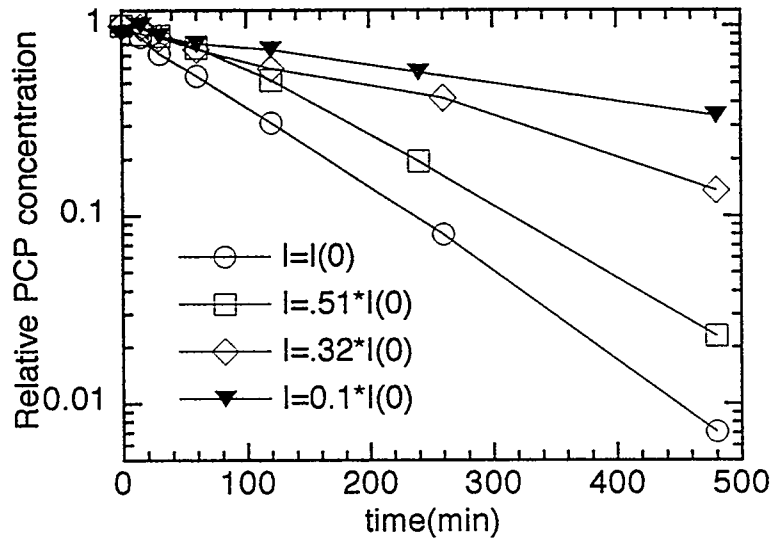
Wilcoxon, Fig, 10



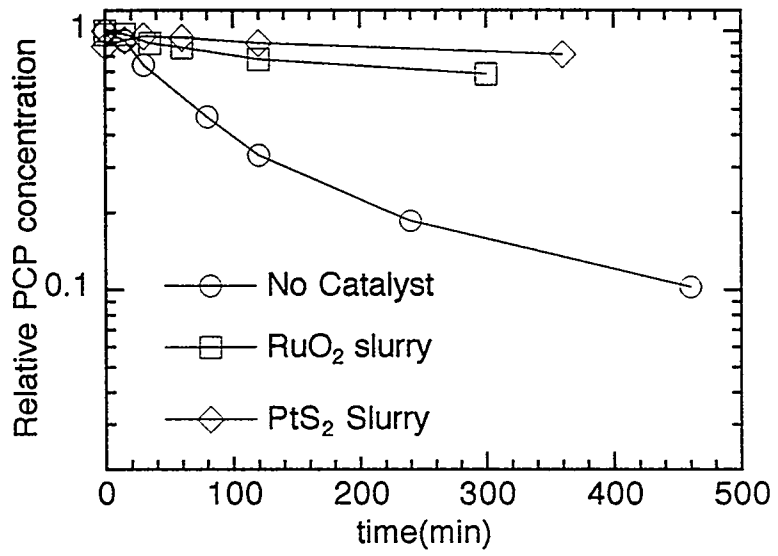
Wilcoxon, Fig. 11



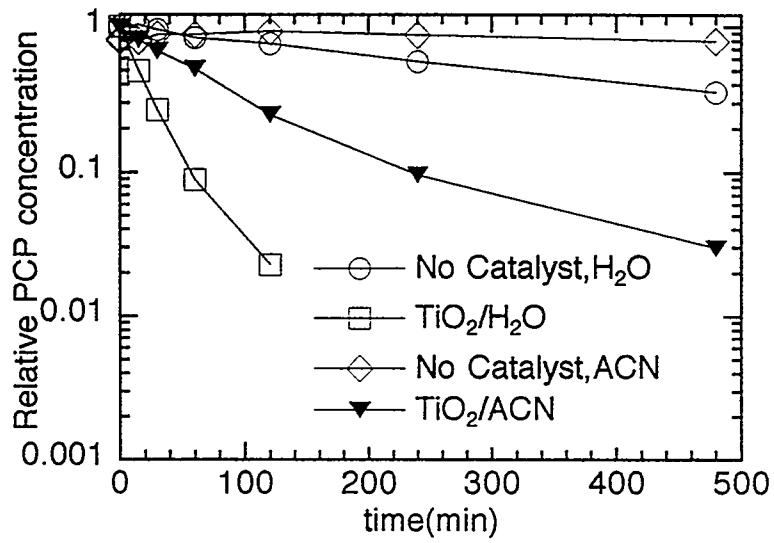
Wilcoxon, Fig. 12



Wilcoxon, Fig. 13



Wilcoxon, Fig. 14



Wilcox; Fig. 15

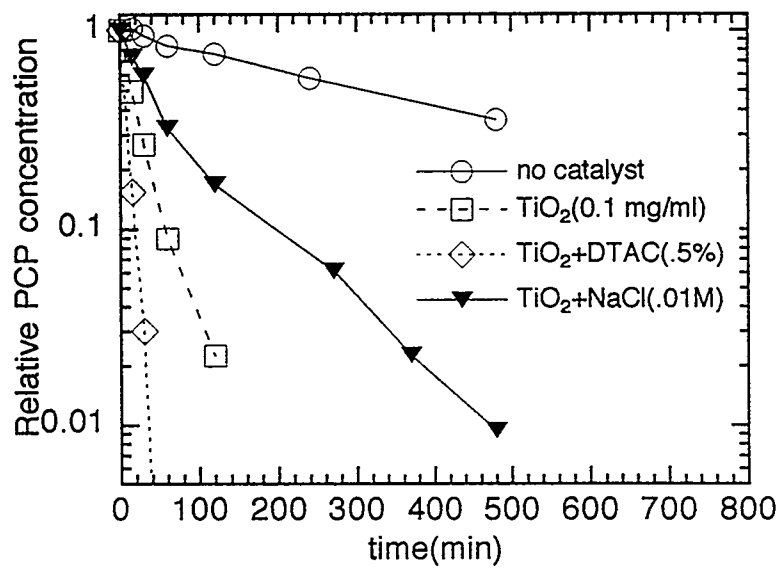


Fig 16, Wilcox

